Spatio-temporal encoding by quadratic gradients in magnetic resonance imaging

Sina Marhabaie, Geoffrey Bodenhausen, Philippe Pelupessy

Spatio-temporal encoding by quadratic gradients in magnetic resonance imaging

Sina Marhabaie[1], Geoffrey Bodenhausen[1], Philippe Pelupessy[1]

[1]Laboratoire des biomolécules, LBM, Département de chimie, École normale supérieure, PSL University, Sorbonne Université, CNRS, 75005 Paris, France

Correspondence to: philippe.pelupessy@ens.fr

Abstract. Spatio-temporal encoding (SPEN) MRI is a non-Fourier imaging technique that encodes the spatial information in such a way that there is a direct relation between the signal intensity recorded during the acquisition and the spin density at a given position. In current spatio-temporal encoding methods, the first crucial step requires imparting a quadratic phase onto the transverse magnetization. Usually, this is achieved by simultaneous application of a frequency-swept (chirp) pulse and a linear magnetic field gradient. In this work, we show that a quadratic phase can be imparted by using quadratic encoding gradients. This leads to smaller specific absorption rates (SARs). Furthermore, the proposed sequence can be used for multi-slice applications similar to ordinary multi-slice sequences, but without the limitations of traditional SPEN.

Introduction

Most conventional MRI methods are based on Fourier transformations: data points are sampled in *k*-space, and the image is obtained by a multi-dimensional Fourier transformation [1]. Spatial encoding, also known as spatio-temporal encoding or SPEN [2,3] is based on sequential excitation or inversion of the spins, and sequential detection of the signals. In order to reconstruct the image it is sufficient to arrange the signals in chronological order of detection without the need for Fourier transformation. So far, a variety of spatio-temporal encoding techniques have been described [2–11]. In most methods, spatial encoding is achieved by simultaneous application of a linear gradient and a frequency-swept (chirp) pulse. This leads to a quadratic phase profile [12,13] where the magnetization vectors of all

voxels are de-phased except for those that lie near the vertex (the flat region) of the quadratic profile. An image can be obtained by shifting the position of the vertex with a linear gradient.

To obtain a satisfactory resolution (especially when no super-resolution methods are used for image reconstruction) and to suppress distortions due to field inhomogeneities, long chirp pulses with large bandwidths are required, because the larger the time-bandwidth [3,7] product (which is a dimensionless parameter obtained by multiplying the duration of the chirp pulse and its bandwidth), the better the resolution. Unfortunately, chirp pulses with large bandwidths lead to large specific absorption rates (SAR). The use of long chirp pulses will also prolong the echo time TE of the sequence with concomitant signal losses. The situation is exacerbated in multi-slice experiments and in sequences that use 180˚chirp pulses [2,6,9,10], as these pulses lead to much higher SARs compared to 90˚chirp pulses. Moreover, in multi-slice experiments, the chirp pulses affect the spins of the whole object and are not limited to the selected slice.

These problems can be avoided by generating a quadratic phase profile with a gradient coil that produces a quadratic magnetic field profile. Of course, linear gradients are still needed for slice selection, *k*-encoding, etc. Non-linear gradients have been proposed for slice selection in Fourier MRI as early as 45 years ago [14]. Different aspects of non-linear encoding fields in MRI have been discussed extensively, and suitable pulse sequences and image reconstruction methods have been published [15–24]. The spatio-temporal dependence of MRI signals encoded with non-linear gradients was previously noted [25], although not in the context of SPEN.

To the best of our knowledge, quadratic encoding gradients have not yet been applied to spatio-temporal encoding (SPEN) methods that usually employ chirp pulses. This paper shows a proof-of-concept to demonstrate that SPEN images can be obtained with quadratic gradients without any chirp pulses. We show that the images obtained by our method (Figures 2-4) have similar properties as traditional SPEN images, and thus can be considered to constitute a class of SPEN images. In addition, we show that quadratic encoding gradients can reduce SAR. This could also allow for shorter echo

times, thus reducing the losses due to relaxation. Moreover, in some circumstances, one could apply linear gradients, for de-phasing or slice refocusing, simultaneously with the quadratic ones.

Theory

Figure 1 shows three sequences with *k*-encoding in one direction and spatio-temporal encoding in the other. Figure 1(a) is a hybrid of spatio-temporal encoding and phase encoding, while Figure 1(b) combines spatio-temporal encoding and frequency encoding. In both cases, *k*-encoding is performed with linear gradients, while spatio-temporal encoding is achieved with quadratic and linear gradients. Ideally, one should have a pulsed quadratic encoding gradient that can be gated on and off during the sequence. However, our experiments were performed with a continuous quadratic gradient provided by a shim coil that cannot be gated. In the ideal case of Figure 1(a), where the quadratic encoding gradient is only applied during the interval τ between excitation and acquisition, the phase of the magnetization at time *t* after starting signal acquisition can be described by:

$$\varphi = \beta z^2 + k_z^{se}(t) z \qquad (1)$$

where $\beta = 2\pi\gamma\alpha\tau$ is the coefficient of the quadratic term, γ is the gyromagnetic ratio, α and τ are the amplitude and duration of the quadratic encoding gradient, *z* is the coordinate along the spatial encoding (*se*) direction, and $k^{se}{}_z(t)$ is the *k*-space coordinate in this dimension at time *t* after starting acquisition. Since the phase of the magnetization varies steeply as a function of the *z* coordinate in all parts of the sample except near the vertex of the quadratic profile [26,27], where $d\varphi/dz \approx 0$, the signal originates almost exclusively from voxels around this vertex. When $k^{se}{}_z(t)$ changes, the position $z(t)$ of the vertex is shifted in proportion:

$$\frac{d\varphi}{dz} = 2\beta z(t) + k_z^{se}(t) = 0 \Rightarrow z(t) = \frac{-k_z^{se}(t)}{2\beta} \qquad (2)$$

thus the field of view (FOV) in the spatial encoding dimension is:

$$FOV_{spatial\ encoding} = \frac{\Delta k_z^{se}}{2\beta} \qquad (3)$$

where $\Delta k^{se}{}_z$ is the relevant range of *k*-space coordinates. As a result, the signal provides a map of the object in the spatial encoding direction, without Fourier transformation. Similar equations can be

obtained for the sequence of Figure 1(b), with the difference that k^{se}_z is constant for each individual scan, while it varies between different scans. The signals are then arranged in a 2D array and a 1D Fourier transformation is performed in the *k*-encoded direction. A single-shot experiment is shown in Figure 1(c). It resembles a gradient echo EPI experiment with an additional quadratic encoding gradient.

In our experiments we have used a shim coil with a current that is applied continuously to generate a quadratic encoding gradient. The presence of this gradient in the excitation period only causes some minor de-phasing and slice deformation (a maximum deviation of 0.24 mm at the corners of the object for the maximum value of $\alpha = 0.45$ T.m^{-2}, and a slice selection gradient of 0.5 T.m^{-1}, which does not occur if one uses switchable quadratic gradients). However, during the signal acquisition a mis-registration of the voxels in the spatio-temporal encoding direction (i.e., in the vertical direction of our images) will occur with respect to the outcome of Equation 2. If the quadratic gradient could be gated off prior to signal acquisition, this voxel mis-registration would not occur, so that successive data points of the spatially encoded signal would correspond to equally spaced points in the image (i.e., in real physical space). Mis-registration means that data points are not equally spaced in the image. Knowledge of the experimental parameters allows one to make a correction. For multi-shot images this mis-registration is negligible because the acquisition time is much shorter than the evolution time. For single-shot experiments this effect needs to be taken into account. Due to mis-registration, the real FOV is smaller than it would be in the ideal case. Furthermore, the centre of the real FOV does not coincide with the centre of the linear gradient coil. It is worth noting that, in our experiments we have calibrated the amplitude of our z^2 shim by estimating a value for the parameter α so that the theoretical equations predict the experimental values observed for FOVs.

One can define a spatio-temporal bandwidth bw_{se} of our experiment as follows; we consider a conventional SPEN experiment with a 180˚ chirp whose duration (τ) is the same as the one of our quadratic gradient and which produces an identical phase profile. The phase profile of such an experiment can be found, for example, in equation 20 of reference 27. Equalising the coefficients of the quadratic term of the traditional experiment with the quadratic term of the experiments that we performed, gives:

$$\frac{\gamma\, G\, \tau}{FOV_{se}} = \frac{bw_{se}\, \tau}{(FOV_{se})^2} = \gamma\, \alpha\, \tau \qquad (4)$$

Hence:

$$bw_{se} = \gamma\, \alpha\, FOV_{se}{}^2 \qquad (5)$$

Methods

Our experiments have been carried out on a Bruker 800 MHz NMR spectrometer equipped with a 25 mm micro-imaging probe, and a Bruker "Micro 2.5" gradient system with maximum switchable linear gradient of 1.0 $T.m^{-1}$. The phantom was a dumbbell-shaped piece of plastic that was placed in a 25 mm outer diameter plastic tube filled with de-ionized water. The pulse programmes were written and implemented using the Paravision programme (version 6.0.1), and the data were processed either by a modified processing algorithm in Paravision or by a home-written Python code. The corrections for the above-mentioned mis-registration were implemented using a home-written Python code. In all experiments, a slice parallel to the *YZ* plane (at $X = 0$) with a thickness of about 0.7 mm was selected by using a linear gradient and a shaped *rf* pulse, the vertical *z* axis being parallel to the main static field. Experimental parameters like the strength of the quadratic gradients and their duration are given in the figure captions.

Results and discussion

The top row in Figure 2 shows an image resulting from the multi-shot SPEN sequence of Figure 1(a). The amplitude of the quadratic encoding (shim) gradient increases from panel a to panel c, resulting in a decreasing FOV in the vertical *z* dimension, in accordance with Equation 2, and also an improving resolution from panel a to panel c. In the sequence of Figure 1(a), the quadratic encoding gradient can also be treated as an inhomogeneous contribution to the static field. Under such conditions, the usual principles of Fourier MRI are applicable, and one can apply a 2D Fourier transform to the raw data.

These images are shown in the bottom row of Figure 2. Of course, in this case, the vertical FOV is not determined by the amplitude of the quadratic encoding gradient, but by the parameters that govern the FOV in Fourier MRI, i.e., by the duration and amplitude of the linear gradients.

Some SPEN images obtained with the sequence of Figure 1(b) under the same conditions as Figure 2 are shown in Figure 3. While Figure 1(a) is a hybrid of spatio-temporal encoding and phase encoding, Figure 1(b) is a hybrid of spatio-temporal encoding and frequency encoding. The top rows of Figures 2 and 3 are quite similar. (There is a slight curvature on the left part which is a bit more pronounced in Figure 3. This could be due to the presence of the continuous quadratic gradient or to effects of other field inhomogeneities). Although the phantom extends beyond the vertical FOV, no aliasing is seen in Figure 2, since the z dimension is spatially encoded, and no Fourier transformation is applied in this direction. Thus, aliasing cannot occur. Aliasing is also absent in the bottom row of Figure 2, despite a 2D Fourier transformation of the raw data, since the signals stemming from areas located beyond the FOV have been removed by digital filtering. In the top row of Figure 3, no aliasing occurs, for the same reason as in the top row of Figure 2. However, aliasing occurs in the images in the bottom row, since the z dimension is phase-encoded and signals originating beyond the FOV are not eliminated by filtration.

Four single-shot SPEN images obtained with the pulse sequence of Figure 1(c) are shown in Figure 4. The quadratic encoding gradient is stronger in Figure 4(b) than in Figure 4(a). Consequently, the FOV is smaller, and the resolution is improved. The amplitude of the quadratic encoding gradient is the same in Figures 4(c), 4(a), and 4(d), but the strength of the “blip” decoding gradients (shown in the pulse programme of Figure 1(c)) has been increased respectively. In 4(c) the strength of the blip gradients is half of 4(a), while in 4(d) it is twice as large as in 4(a). Consequently, the FOV in the spatio-temporal encoding direction in 4(c) is halved compared to 4(a), while in 4(d) it is doubled. As explained in the Theory section, a mis-registration occurs due to the presence of the quadratic gradient throughout the detection interval. This mis-registration has been compensated by a method described in the supporting information, which also shows a multi-shot reference image, and an EPI image for the sake of comparison.

Conclusions

The effect of various experimental parameters on the images has been investigated in Figures 2-4. Quadratic encoding gradients can lead to a comparable phase profile as the simultaneous application of a chirp pulse and a linear gradient. Hence, it shares the same advantages (notably its resilience to inhomogeneous static magnetic fields B_0) and disadvantages, notably losses in SNR. These losses might be mitigated by using super-resolution reconstruction methods [3,5]. In contrast to traditional SPEN, quadratic encoding gradients allow one to achieve an increased resolution and a better resilience to inhomogeneous B_0 fields without increasing the SAR. Moreover, since (as in FT MRI) the *rf* pulses only affect a chosen slice, multi-slice applications can be realised more easily. The quality of the images shown in this work suffers (most likely) from the fact that the quadratic gradient could not be gated during the pulse sequence. Moreover, the z^2 shim coil that has been used generates a gradient described by the following equation [28]:

$$B_z \propto 2z^2 - (x^2 + y^2) \qquad (6)$$

In a slice parallel with the YZ plane centred on a value x_0, the term x^2 is constant, but the y^2 term leads to some distortions in our images. For this method to become competitive, MRI scanners would need to be equipped, in addition to three standard linear pulsed field gradients, with quadratic pulsed field gradients, which would probably need a significant technological development. Only after performing our method with such a gradient system, and checking whether nerve stimulation effects are different from those induced by linear gradients, a meaningful and thorough comparison with different variants of conventional SPEN techniques (i.e., with 90° or 180° chirp pulses) can be made. Furthermore, using spin echoes to refocus field inhomogeneities and super-resolution reconstruction techniques merit further investigation since they could ameliorate this work.

Acknowledgments

The authors acknowledge financial support of the European Research Council (ERC, project 339754 "Dilute para-water"), the Equipex programme "Paris en Résonance", and the support of GIS-IBISA programme of the IMACHEM imaging platform (École Normale Supérieure – Collège de France).

References:

[1] R.W. Brown, Y.-C.N. Cheng, E.M. Haacke, M.R. Thompson, R. Venkatesan, Magnetic Resonance Imaging: Physical Principles and Sequence Design, Second Ed., John Wiley & Sons, Inc., Hoboken, New Jersey, 2014.

[2] R. Schmidt, B. Baishya, N. Ben-Eliezer, A. Seginer, L. Frydman, Super-resolved parallel MRI by spatiotemporal encoding, Magn. Reson. Imaging. 32 (2014) 60–70. doi:10.1016/j.mri.2013.07.007.

[3] N. Ben-Eliezer, Y. Shrot, L. Frydman, D.K. Sodickson, Parametric analysis of the spatial resolution and signal-to-noise ratio in super-resolved spatiotemporally encoded (SPEN) MRI, Magn. Reson. Med. 72 (2014) 418–429. doi:10.1002/mrm.24954.

[4] J.-K. Ryu, S. Han, S.-H. Oh, J. Lee, S.-G. Kim, J.-Y. Park, A new ultrafast 3D gradient echo-based imaging method using quadratic-phase encoding, Magn. Reson. Med. 82 (2019) 237–250. doi:10.1002/mrm.27711.

[5] N. Ben-Eliezer, M. Irani, L. Frydman, Super-resolved spatially encoded single-scan 2D MRI, Magn. Reson. Med. 63 (2010) 1594–1600. doi:10.1002/mrm.22377.

[6] Z. Zhang, A. Seginer, L. Frydman, Single-scan MRI with exceptional resilience to field heterogeneities, Magn. Reson. Med. 77 (2016) 1–12. doi:10.1002/mrm.26145.

[7] R. Chamberlain, J.-Y. Park, C. Corum, E. Yacoub, K. Ugurbil, C.R. Jack, M. Garwood, RASER: A new ultrafast magnetic resonance imaging method, Magn. Reson. Med. 58 (2007) 794–799. doi:10.1002/mrm.21396.

[8] U. Goerke, M. Garwood, K. Ugurbil, Functional magnetic resonance imaging using RASER, Neuroimage. 54 (2011) 350–360. doi:10.1016/j.neuroimage.2010.08.011.

[9] T. Zhang, L. Chen, J. Huang, J. Li, S. Cai, C. Cai, Z. Chen, Ultrafast multi-slice spatiotemporally encoded MRI with slice-selective dimension segmented, J. Magn. Reson. 269 (2016) 138–145. doi:http://dx.doi.org/10.1016/j.jmr.2016.06.002.

[10] L. Ciobanu, E. Solomon, N. Pyatigorskaya, T. Roussel, D. Le Bihan, L. Frydman, fMRI contrast at high and ultrahigh magnetic fields: Insight from complementary methods, Neuroimage. 113 (2015) 37–43. doi:10.1016/j.neuroimage.2015.03.018.

[11] S. Marhabaie, G. Bodenhausen, P. Pelupessy, Susceptibility contrast by echo shifting in spatially encoded single-scan MRI, Phys. Chem. Chem. Phys. 19 (2017) 14210–14213. doi:10.1039/C7CP01898C.

[12] J.G. Pipe, Spatial Encoding and Reconstruction in MRI with Quadratic Phase Profiles, Magn. Reson. Med. 33 (1995) 24–33. doi:10.1002/mrm.1910330105.

[13] J.G. Pipe, Analysis of localized quadratic encoding and reconstruction, Magn. Reson. Med. 36 (1996) 137–146. doi:10.1002/mrm.1910360122.

[14] A. Kumar, D. Welti, R.R. Ernst, NMR Fourier zeugmatography, J. Magn. Reson. 18 (1975) 69–83. doi:https://doi.org/10.1016/0022-2364(75)90224-3.

[15] G. Galiana, J.P. Stockmann, L. Tam, R.T. Constable, Spin dephasing under nonlinear gradients: Implications for imaging and field mapping, Magn. Reson. Med. 67 (2012) 1120–1126. doi:10.1002/mrm.23085.

[16] D. Gallichan, C.A. Cocosco, A. Dewdney, G. Schultz, A. Welz, J. Hennig, M. Zaitsev, Simultaneously driven linear and nonlinear spatial encoding fields in MRI, Magn. Reson. Med. 65 (2011) 702–714. doi:10.1002/mrm.22672.

[17] K.J. Layton, D. Gallichan, F. Testud, C.A. Cocosco, A.M. Welz, C. Barmet, K.P. Pruessmann, J. Hennig, M. Zaitsev, Single shot trajectory design for region-specific imaging using linear and nonlinear magnetic encoding fields, Magn. Reson. Med. 70 (2013) 684–696. doi:10.1002/mrm.24494.

[18] J.P. Stockmann, P.A. Ciris, G. Galiana, L. Tam, R.T. Constable, O-space imaging: Highly efficient parallel imaging using second-order nonlinear fields as encoding gradients with no phase encoding, Magn. Reson. Med. 64 (2010) 447–456. doi:10.1002/mrm.22425.

[19] J.P. Stockmann, G. Galiana, L. Tam, C. Juchem, T.W. Nixon, R.T. Constable, In vivo O-Space imaging with a dedicated 12 cm Z2 insert coil on a human 3T scanner using phase map calibration, Magn. Reson. Med. 69 (2013) 444–455. doi:10.1002/mrm.24282.

[20] E.X. Wu, G. Johnson, S.K. Hilal, Z.-H. Cho, A new 3D localization technique using quadratic field gradients, Magn. Reson. Med. 32 (1994) 242–245. doi:10.1002/mrm.1910320214.

[21] J. Hennig, A.M. Welz, G. Schultz, J. Korvink, Z. Liu, O. Speck, M. Zaitsev, Parallel imaging in non-bijective, curvilinear magnetic field gradients: a concept study, Magn. Reson. Mater. Physics, Biol. Med. 21 (2008) 5. doi:10.1007/s10334-008-0105-7.

[22] G. Schultz, P. Ullmann, H. Lehr, A.M. Welz, J. Hennig, M. Zaitsev, Reconstruction of MRI data encoded with arbitrarily shaped, curvilinear, nonbijective magnetic fields, Magn. Reson. Med. 64 (2010) 1390–1403. doi:10.1002/mrm.22393.

[23] K.J. Layton, M. Morelande, P.M. Farrell, B. Moran, L.A. Johnston, Performance Analysis for Magnetic Resonance Imaging With Nonlinear Encoding Fields, IEEE Trans. Med. Imaging. 31 (2012) 391–404. doi:10.1109/TMI.2011.2169969.

[24] Y. Xu, H. Tian, Z. Zhu, G. Zhang, Y. Chang, R. Jiang, X. Wang, X. Yang, MRI image reconstruction under linear and hyperbolic gradients, in: 2013 1st Int. Conf. Orange Technol., 2013: pp. 139–142.

doi:10.1109/ICOT.2013.6521177.

[25] M. Zaitsev, G. Schultz, J. Hennig, R. Gruetter, D. Gallichan, Parallel imaging with phase scrambling, Magn. Reson. Med. 73 (2015) 1407–1419. doi:10.1002/mrm.25252.

[26] R. Paquin, P. Pelupessy, G. Bodenhausen, Cross-encoded magnetic resonance imaging in inhomogeneous fields, J. Magn. Reson. 201 (2009) 199–204. doi:10.1016/j.jmr.2009.09.008.

[27] A. Tal, L. Frydman, Spatial encoding and the single-scan acquisition of high definition MR images in inhomogeneous fields, J. Magn. Reson. 182 (2006) 179–194. doi:10.1016/j.jmr.2006.06.022.

[28] G.N. Chmurny, D.I. Hoult, The Ancient and Honourable Art of Shimming, Concepts Magn. Reson. 2 (1990) 131–149. doi:10.1002/cmr.1820020303.

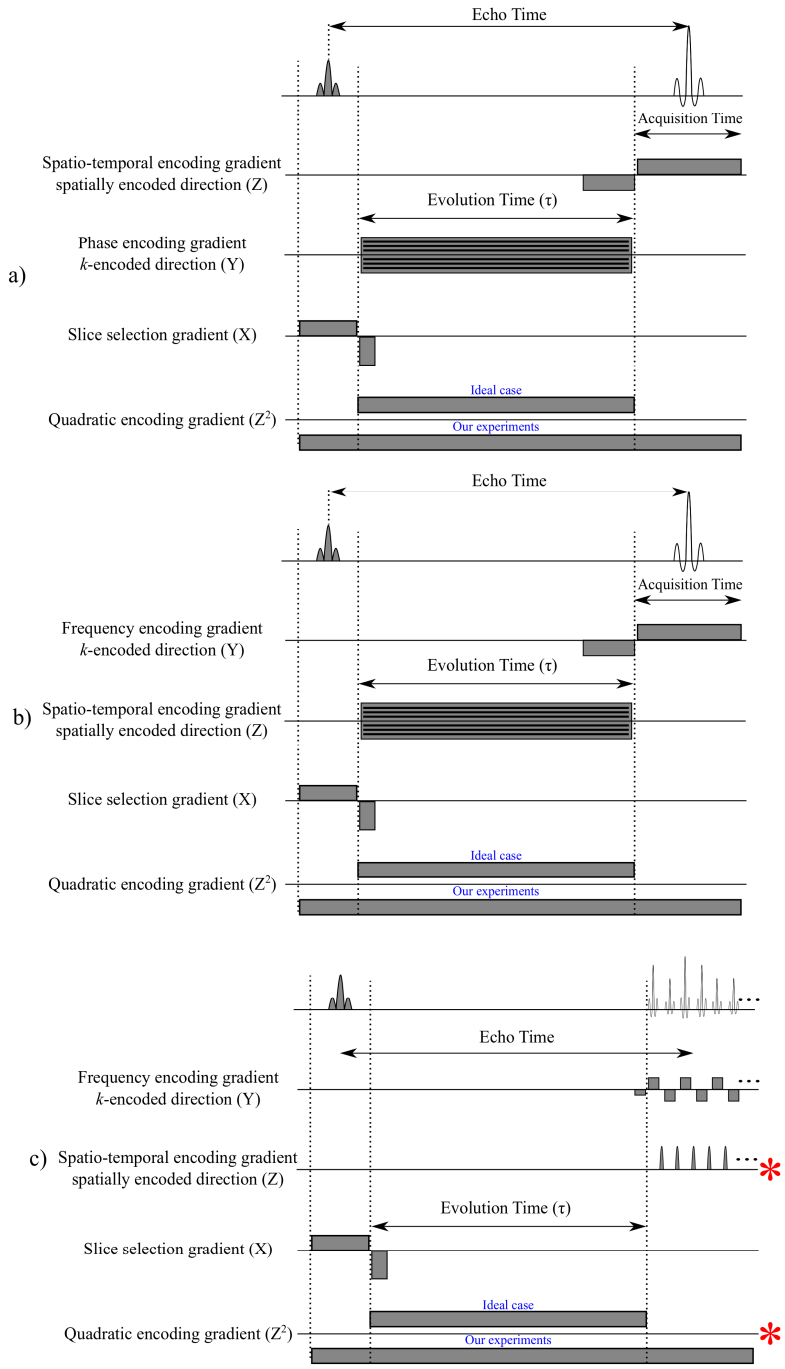

255 Figure 1: Multi-shot and single-shot spatio-temporal encoding sequences used in this work. Slice selection and *k*-encoding are performed by linear gradients like in Fourier imaging sequences. Spatio-temporal encoding is achieved using a quadratic, and linear blipped gradients. Note that, in contrast to conventional SPEN methods, no chirp pulse is used in this method.

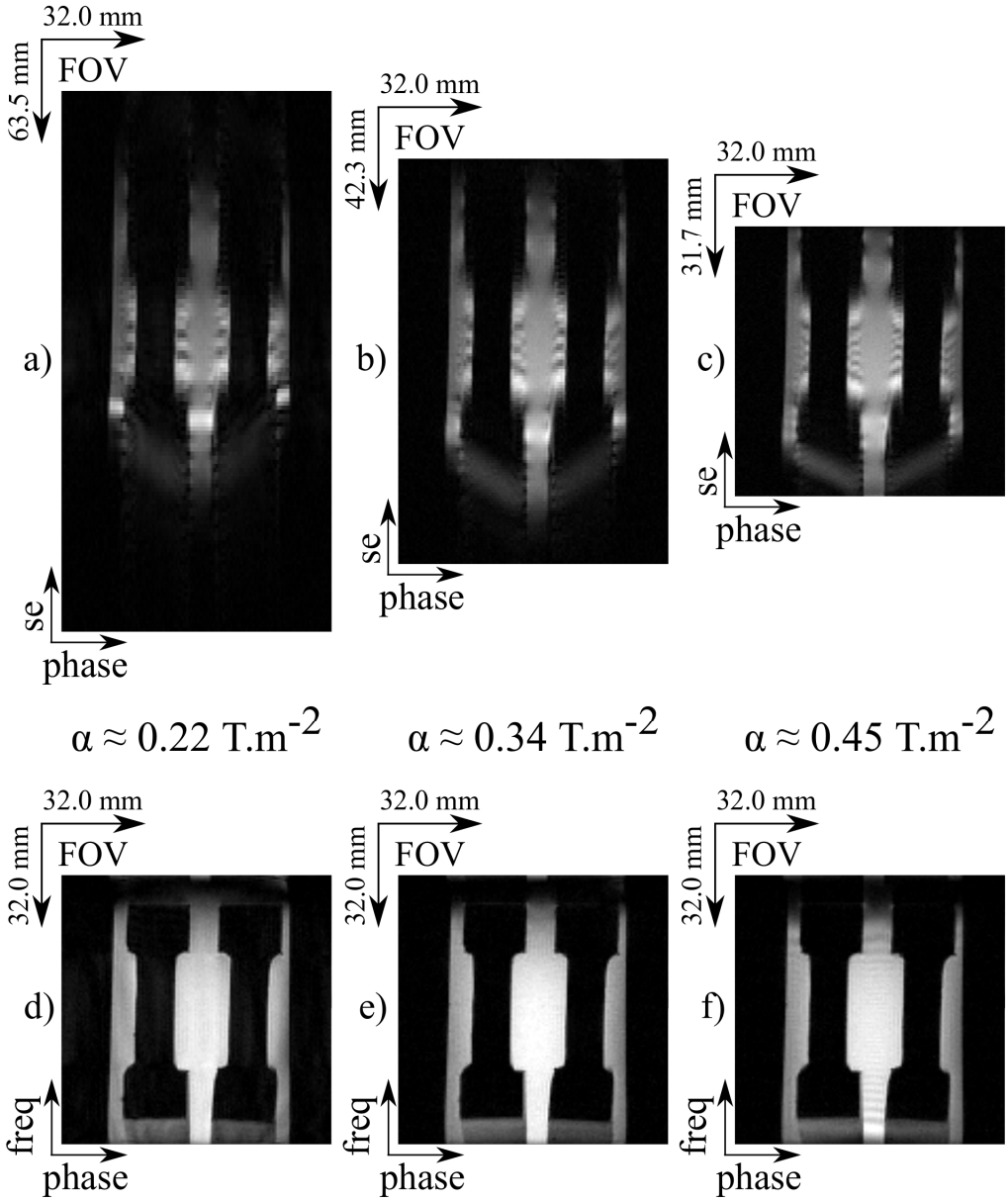

Figure 2: Top row: three SPEN images obtained by the multi-shot sequence of Figure 1 (a), using a quadratic encoding gradient, with the following parameters: matrix size 128 × 128, TE = 3.3 ms, flip angle 30°, TR = 100 ms, and readout bandwidth bw = 500 kHz. In (a) the amplitude of the quadratic encoding gradient was $\alpha \approx 0.22$ T.m^{-2} (corresponding to a bw_{se} = 38.6 kHz) and the FOV = 63.5 × 32.0 mm; in (b) $\alpha \approx 0.34$ T.m^{-2} (corresponding to a bw_{se} = 25.7 kHz) and the FOV = 42.3 × 32.0 mm; and in (c) $\alpha \approx 0.45$ T.m^{-2} (corresponding to a bw_{se} = 19.3 kHz) and FOV = 31.7 × 32.0 mm. These images result from hybrids of spatio-temporal encoding (along the vertical z axis) and phase encoding (along the horizontal y axis). Increasing the amplitude of the quadratic encoding gradient will decrease the FOV in the spatio-temporal encoding direction. Bottom row: (d, e, and f) images obtained by applying a Fourier transformation also in the vertical direction (2D FT) on the same raw data as the top row. (d) Raw data of image (a); (e) raw data of image (b); (f) raw data of image (c). For all bottom row images, the FOV was 32.0 × 32.0 mm.

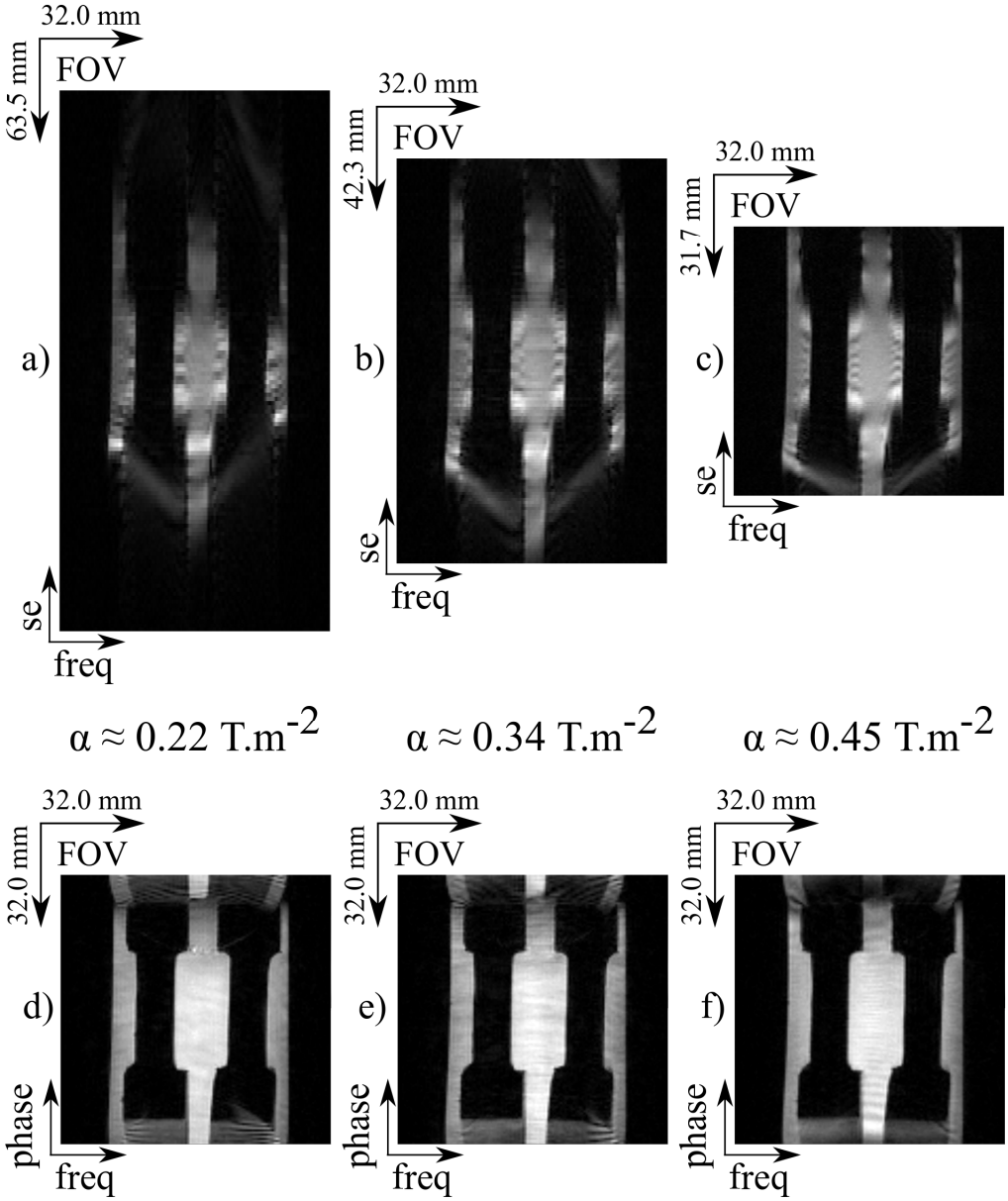

Figure 3: Top row: three SPEN images obtained with the multi-shot sequence of Figure 1(b), using a quadratic encoding gradient, with the following parameters: matrix size 128 × 128, TE = 3.3 ms, flip angle 30˚, TR = 100 ms, and readout bandwidth bw = 500 kHz. In (a) the amplitude of the quadratic encoding gradient was $\alpha \approx 0.22\ \mathrm{T.m^{-2}}$ (corresponding to a bw_{se} = 38.6 kHz) and FOV = 63.5 × 32.0 mm; in (b) $\alpha \approx 0.34\ \mathrm{T.m^{-2}}$ (corresponding to a bw_{se} = 25.7 kHz) and FOV = 42.3 × 32.0 mm; and in (c) $\alpha \approx 0.45\ \mathrm{T.m^{-2}}$ (corresponding to a bw_{se} = 19.3 kHz) and FOV = 31.7 × 32.0. These images are hybrids of spatio-temporal encoding (along the vertical z axis) and frequency encoding (along the horizontal y axis). Increasing the amplitude of the quadratic encoding gradient leads to a decrease of the FOV in the spatio-temporal encoding direction. Bottom row: (d, e, and f) images obtained by applying a Fourier transformation also in the vertical direction (2D FT) on the same raw data as the top row. (d) Raw data of image (a); (e) raw data of image (b); (f) raw data of image (c). For all bottom row images, the FOV was 32.0 × 32.0. Aliasing is evident in three images of the bottom row.

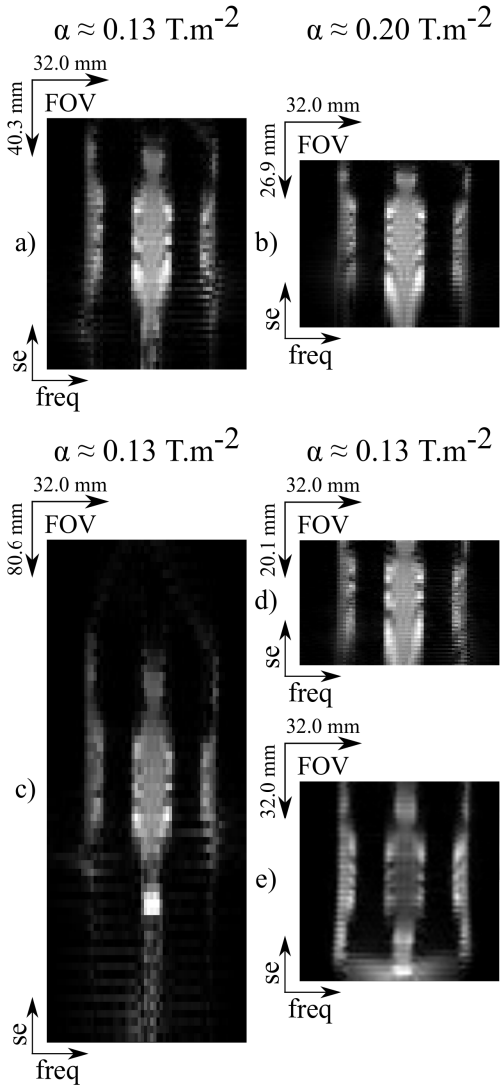

Figure 4, panels (a) to (d): Single-shot SPEN images obtained with the sequence shown in Figure 1(c). The experiments have been performed with different values of quadratic and linear blip gradients (indicated with red stars in Figure 1(c)), and with the following parameters: matrix size 64 × 64, TE = 7.2 ms, flip angle 90°, evolution time τ = 2.66 ms, and readout bandwidth bw = 652 kHz. In (a) the amplitude of the quadratic encoding gradient pulse was $\alpha \approx 0.13$ T.m^{-2} (corresponding to a bw_{se} = 9.3 kHz), and FOV = 40.3 × 32.0 mm; in (b) $\alpha \approx 0.20$ T.m^{-2} (corresponding to a bw_{se} = 6.2 kHz), and the FOV was 26.9 × 32.0 mm; in (c) $\alpha \approx 0.13$ T.m^{-2} (corresponding to a bw_{se} = 37.2 kHz), and FOV = 80.6 × 32.0 mm; in (d) $\alpha \approx 0.13$ T.m^{-2} (corresponding to a bw_{se} = 2.3 kHz), and FOV = 20.1 × 32.0 mm. These images are hybrids of spatio-temporal encoding (along the vertical z axis) and frequency encoding (along the horizontal y axis). Increasing the amplitude of the quadratic encoding gradient will decrease the FOV in the spatio-temporal encoding direction. Conversely, increasing the amplitude of the linear blip gradient will increase the FOV in the spatio-temporal encoding direction. Note that there is a non-negligible mis-registration of the voxels. The images have been corrected to compensate for this effect. Panel (e): for comparison, a traditional single-shot SPEN image obtained by the RASER [7] sequence (using a chirp pulse and linear gradient), with the following parameters: matrix size 64 × 64, TE = 37.8 ms, FOV = 32.0 × 32.0 mm, flip angle 90°, chirp pulse duration = 9.08 ms, readout bandwidth 652 kHz, and spatio-temporal encoding bandwidth bw_{se} = 7.8 kHz.

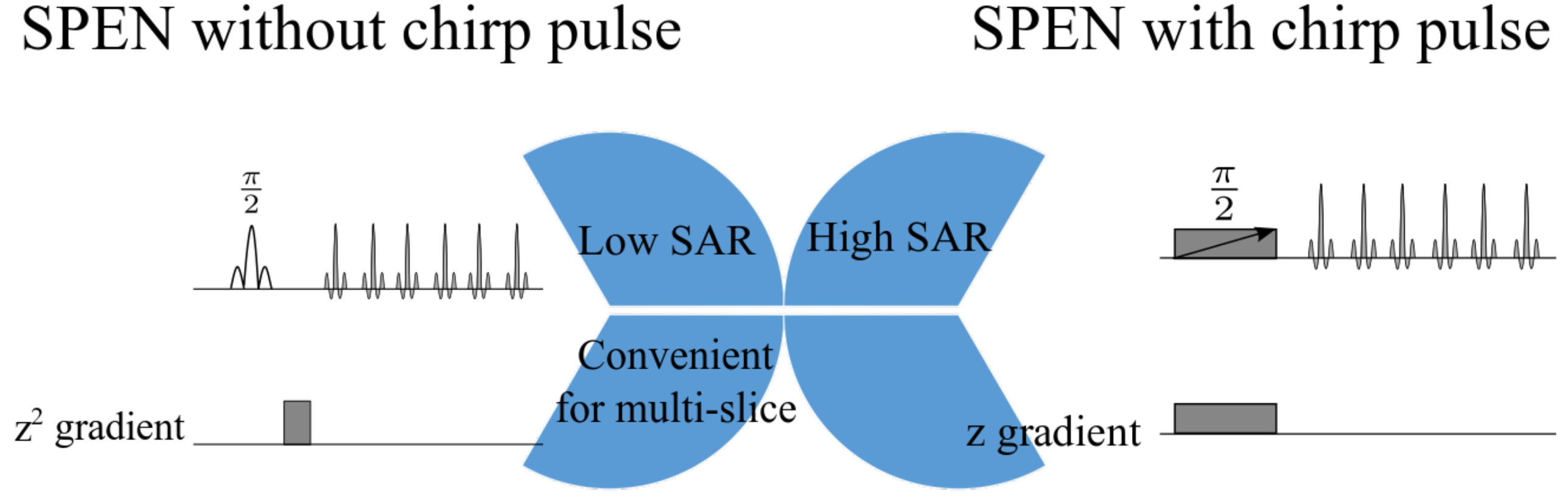
SPEN without chirp pulse
SPEN with chirp pulse
π/2
π/2
Low SAR
High SAR
Convenient
for multi-slice
z² gradient
z gradient